Available online at www.sciencedirect.com

ScienceDirect

Procedia Structural Integrity 52 (2024) 740–751

Structural Integrity Procedia

www.elsevier.com/locate/procedia

Fracture, Damage and Structural Health Monitoring

Numerical recipes of virtual element method for phase field modeling of brittle fracture

Tong-Rui Liu[a,*], Fadi Aldakheel[b], M. H. Aliabadi[a]

[a]*Structural Integrity & Health Monitoring Group, Department of Aeronautics, Imperial College London, SW7 2AZ, London, UK*
[b]*Institut für Baumechanik und Numerische Mechanik, Leibniz Universität Hannover, Appelstraße 9A, 30167 Hannover,Germany*

Abstract

In this work, a new and efficient virtual element formulation for *non-standard* phase field model of brittle fracture is presented. A multi-pass alternative minimization solution scheme based on algorithm operator splitting is utilized, which decouples the whole problem into two parts, namely, mechanical and damage sub-problems. The former is treated as elasto-static problem, while the latter one is treated as Poisson-type of reaction-diffusion equation subjected to bounded and irreversibility constraint. To demonstrate the performance of proposed formulation, several benchmark problems are studied and results are in good agreement with corresponding finite element calculations and experimental studies.

Keywords: Brittle fracture; Damage mechanics; Phase field method; Virtual element method;

1. Introduction

Fracture is a one of the most common failure modes in engineering materials and structures. The prevention of fracture becomes a major concern in engineering design and structural analysis. During the past few decades, researchers proposed several pathways for analysis of fracture behaviors, which mainly can be generalized into three categories: theoretical, experimental and computational approaches.

Computational fracture and damage mechanics becomes an indispensable tool for predicting complex crack patterns in solids and structures. Broadly speaking, the modeling of fracture and damage behaviors can be classified into two families, i.e., continuity (smeared) and discontinuity (discrete) approaches De Borst (2022). Recently, a new smeared approach called variational phase field modeling of fracture came into pictures Francfort and Marigo (1998), which is rooted in Griffith's energetic theory of brittle fracture. In this method, the crack path is not set forth straightforward but described by auxiliary indicators, namely, crack phase field variables Bourdin (2000). The crack phase field variables and displacement fields are solved via a global minimization procedure of total energy functional, which includes stored elastic energy, regularized fracture surface energy and external work. The total potential energy is not always convex for displacement field and crack phase field at the same time, which needs special solution techniques to deal with, i.e., alternative minimization (staggered) solver Bourdin (2000). Similar to other continuum damage

* Corresponding author
E-mail address: tongrui.liu18@imperial.ac.uk (T-R. Liu), fadi.aldakheel@ibnm.uni-hannover.de (F. Aldakheel), m.h.aliabadi@imperial.ac.uk (M.H.Aliabadi)

2452-3216
10.1016/j.prostr.2023.12.074

models, the numerical implementation is rather simple and straightforward in *element* based numerical methods, such as finite element method, virtual element method Beirão da Veiga (2013) and finite difference methods, to name a few. Recent years, several phase-field fracture formulations has been proposed for brittle Miehe (2010b), cohesive Wu (2017); Wu and Nguyen (2018), ductile Ambati (2015b), dynamic Borden (2012); Mandal (2020) and multi-physics Miehe (2015a,b); Mandal (2021); Martínez-Pañeda (2018) fracture, interested readers may read the review article Wu (2020) for more details.

From an effective numerical discretization point of view, the common numerical method for phase field modeling of fracture is undoubtedly finite element method (FEM). Recent years, several novel numerical methods came into picture, such as meshfree method (MFM) Belytschko (1994), material point method (MPM) Sulsky (1994) and virtual element method (VEM) Beirão da Veiga (2013), to name a few. As a new and effective numerical method for solving partial different equations (PDEs), the virtual element method evolved from mimetic finite difference (MFD) method, which can be a generalization of finite element method. Unlike FEM, the weak form in such method is decomposed into two parts, namely, consistency and stabilization terms. As its name suggests, the terminology "virtual" means that the calculation of shape functions does not need to access the information inside the element but only use the degree of freedoms (DOFs) Beirão da Veiga (2014). The advantage of VEM over FEM can be generalized as: (1) No Gauss integration is needed for computing the element stiffness matrix, which bypasses the issues of badly approximation for the poor quality of element topology as in (polygonal) finite element method. (2) Arbitrary type element can be used for numerical simulation, including (non-) convex 2D polygonal and 3D polyhedral elements. (3) Adaptive mesh refinement becomes rather simple since the nodes within elements can be altered during the simulation process. Therefore, there is no extra effort to deal with the appearance of hanging nodes when changing the topology of elements as in FEM.

Recently, VEM has been successfully applied to solve fracture mechanics problems. Nguyen-Thanh et al proposed an efficient VEM formulation for solving linear elastic fracture mechanics problems Nguyen-Thanh (2018). Aldakheel et al proposed an efficient virtual element formulation for solving standard (`AT2`) phase field modeling of brittle Aldakheel (2018) and ductile fracture Aldakheel (2019) under quasi-static loading. Hussein et al presented a VEM based cutting technique with adaptive phase field modeling of fracture to predict the crack path in brittle solids Hussein (2020). Liu et al proposed an explicit virtual element formulation for phase field modeling of dynamic fracture Liu (2023).

In this work, a new virtual element formulation for *non-standard* (`AT1`) phase field modeling of brittle fracture is proposed. A multi-pass alternative minimization solution scheme is utilized to decouple the whole problem into two parts, the mechanical and damage sub-problems, which can be solved in a staggered manner. The former is regraded as elasto-static equation Beirão da Veiga (2015), while the latter one is treated as Poisson-type of reaction-diffusion equation Beirão da Veiga (2016) subjected to bounded and irreversibility constraint. The difference in this work from Aldakheel (2018) is outlined in Table 1. Two benchmark problems are prsented, and the results are compared with corresponding FEM calculations and reference results.

Table 1: Difference of setting up in this work from Aldakheel et.al

Setting	This work	Aldakheel (2018)
Time stepping	Multi-pass staggered scheme	One-pass staggered scheme
VEM stabilization scheme	Nodal based stabilization	Hybrid FEM-VEM (Energy-based) stabilization
Damage irreversibility constraint	Bounded constraint optimization solver	History field
Crack geometry function	`AT1`	`AT2`

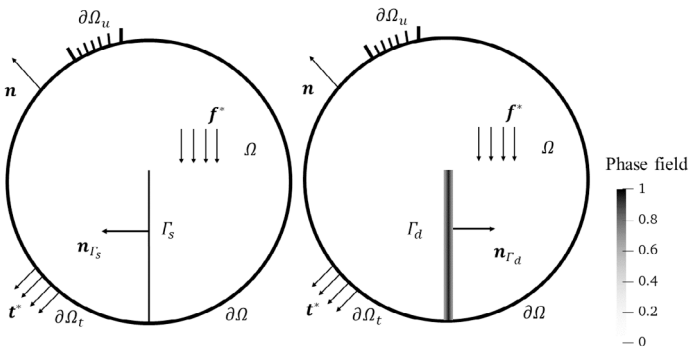

Figure 1: Sketch of solid domain Ω with sharp crack Γ_{s} (left) and its phase field regularized representation Γ_{d} (right)

2. Mathematical foundation

2.1. Phase field model of brittle fracture

As shown in Fig.1, Consider $\Omega \subset \mathbb{R}^{n_{\mathrm{dim}}}$ ($n_{\mathrm{dim}} = 1, 2$) as a solid domain, with its external boundary denoted by $\partial\Omega \subset \mathbb{R}^{n_{\mathrm{dim}}-1}$, the outwards normal unit vector to the external boundary is denoted as $\boldsymbol{n}$. The kinetic and fracture responses at a point $\boldsymbol{x} \in \Omega$ and time $t \in \mathcal{T} = [0, T]$ can be described by admissible displacement $\boldsymbol{u}(\boldsymbol{x}, t)$ and fracture phase field $d(\boldsymbol{x}, t)$:

$$\boldsymbol{u} : \begin{cases} \Omega \times \mathcal{T} \to \mathbb{R}^{n_{\mathrm{dim}}} \\ (\boldsymbol{x}, t) \mapsto \boldsymbol{u}(\boldsymbol{x}, t) \end{cases} \quad \text{and} \quad d : \begin{cases} \Omega \times \mathcal{T} \to [0, 1] \\ (\boldsymbol{x}, t) \mapsto d(\boldsymbol{x}, t) \end{cases} \quad \text{with} \quad \dot{d} \geq 0 \tag{1}$$

where $d(\boldsymbol{x}, t) = 0$ and $d(\boldsymbol{x}, t) = 1$ denote the intact and fully damaged state of the material, respectively. $\dot{\square} = d\square/dt$ represents the time derivative of $\square$. The deformation is measured by the strain field $\boldsymbol{\varepsilon}(\boldsymbol{x}, t) : \Omega \times \mathcal{T} \to [\mathbb{R}^{n_{\mathrm{dim}} \times n_{\mathrm{dim}}}]^{\mathrm{sym}}$ under infinitesimal strain theory, such as:

$$\boldsymbol{\varepsilon} = \nabla^{\mathrm{sym}} \boldsymbol{u} = \mathrm{sym}[\nabla \boldsymbol{u}] := \frac{1}{2} \left[\nabla \boldsymbol{u} + \nabla \boldsymbol{u}^T \right]. \tag{2}$$

The symbol $\nabla^{\mathrm{sym}}(\cdot)$ denotes the symmetric gradient with respect to spatial coordinates. For the phase field problem, as shown in Fig. 1(right), the sharp crack topology Γ_{s} is regularized by a diffusive phase field $d(\boldsymbol{x}) : \Gamma_{\mathrm{d}} \to [0, 1]$ over a localized band $\Gamma_{\mathrm{d}} \subseteq \Omega$ which is unknown a priori, and its exterior domain $\Omega \setminus \Gamma_{\mathrm{d}}$ keeping intact. By introducing the crack surface density function $\gamma(d, \nabla d)$, the sharp crack is regularized by phase field approximation in a purely geometric context as:

$$\underbrace{\int_{\Gamma_{\mathrm{d}}} \psi_c(d, \nabla d) \mathrm{d}V = \int_{\Gamma_{\mathrm{d}}} G_c \, \gamma(d, \nabla d) \mathrm{d}V}_{\text{phase field regularized crack}} \approx \underbrace{\int_{\Gamma_{\mathrm{s}}} G_c \, \mathrm{d}A}_{\text{sharp crack}} \tag{3}$$

where $\psi_c(d, \nabla d)$ is defined as the accumulated dissipative energy density. G_c is introduced as a fracture toughness per unit area and $\gamma(d, \nabla d)$ can be expressed as:

$$\gamma(d, \nabla d) = \frac{3}{8}\left[\frac{d}{l} + l|\nabla d|^2\right] \tag{4}$$

where l represents the characteristic length scale parameter that controls the bandwidth of the phase field. In this work, a non-standard (AT1) phase field model is utilized Pham (2009), which has an elastic stage before damage initiation. The above introduced variables will characterize the brittle failure response of a solid, based on the two global primary fields and three constitutive state variables, such as:

$$\begin{cases}\text{Global primary variables: } \mathfrak{U} := \{\boldsymbol{u}, d\} \\ \text{Constitutive State Variables: } \mathfrak{C} := \{\boldsymbol{\varepsilon}, d, \nabla d\}\end{cases} \tag{5}$$

A mechanical sub-problem and a damage sub-problem can be defined for $\boldsymbol{u}$ and d, respectively. Following the work of Wu (2017); Wu and Nguyen (2018), one can obtain the weak form for $\boldsymbol{u}$ and d, such as:

$$\begin{cases}\displaystyle\int_\Omega \sigma : \nabla^{\text{sym}} \delta\boldsymbol{u} \mathrm{d}V = \delta\mathscr{P} \\ \displaystyle\int_{\Gamma_\mathrm{d}} \left[\mathcal{A}\delta d - G_c \delta\gamma\right] \mathrm{d}V \leq 0\end{cases} \tag{6}$$

where $\mathscr{P}$ is defined as virtual power associated with external body forces and surface tractions. The inequality in Eq.6 represents the irreversibility of phase field d. The constitutive equations for $\boldsymbol{\sigma}$ and $\mathcal{A}$ can be written as:

$$\begin{cases}\boldsymbol{\sigma} := g(d)\hat{\boldsymbol{\sigma}} \\ \mathcal{A} := -g'(d)\hat{\mathcal{A}}\end{cases} \tag{7}$$

where $\hat{\boldsymbol{\sigma}}$ and $\hat{\mathcal{A}}$ represent the effective (undamaged) stress and crack driving force, respectively. For tension dominant failure, one can choose either spectral splitting in Miehe (2010a) or Rankine splitting in Wu (2017) for computing the crack driving force $\hat{\mathcal{A}}$. $g(d)$ represents the energetic degradation function. In this work, only quadratic degradation function $g(d) = (1-d)^2$ is considered.

2.2. Virtual element discretization

In a general 2D polygonal conforming mesh Ω_h with a total number of elements n_E is considered for the discretization of the domain Ω. Each element (need not to be convex) $E \in \Omega_h$ consists of n_V nodes (vertices) and its boundary edge ∂E is defined as e. The symbols h_E and $|E|$ denote the maximum length of the edge and area of an element E, respectively. For $j = 1, 2, ..., n_V$, $\boldsymbol{x}_j$ denotes the initial position vector of nodal coordinate in 2D, such as $\boldsymbol{x}_j = \{x_j, y_j\}$. In each element, the vertexes are indexed counterclockwise as plotted in Fig.2, which represents a pentagon element in 2D. The global virtual spaces for primary variables (displacement, phase field) in Eq.5 can be defined as:

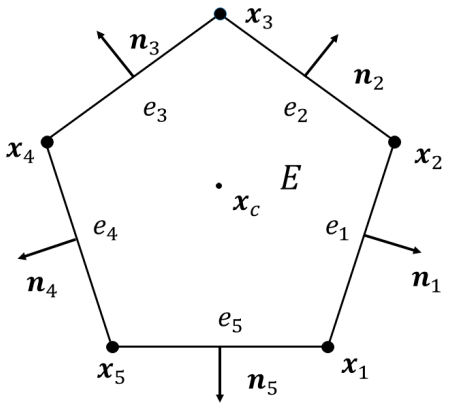

Figure 2: Schematic description of a 2D polygonal element E, $\boldsymbol{x}_c$ is the centroid of E

$$\begin{cases} \text{displacement: } \mathcal{V}_h := \{\boldsymbol{v}_h \in \mathcal{V} : \boldsymbol{v}_{h|E} \in \mathcal{V}_{h|E}, \forall E \in \Omega_h\} \\ \text{phase field: } \mathcal{Q}_h := \{q_h \in \mathcal{Q} : q_{h|E} \in \mathcal{Q}_{h|E}, \forall E \in \Omega_h\} \end{cases} \tag{8}$$

where $\mathcal{V}_{h|E}$ and $\mathcal{Q}_{h|E}$ represent the local virtual space for displacement and phase field, respectively. Following the work of Beirão da Veiga (2013); Gain (2014), a lower order VEM formulation (with linear polynomial) is taken into consideration. For $E \in \Omega_h$, the discrete virtual space $\mathcal{Q}_{h|E}$ at element level is defined as:

$$\mathcal{Q}_{h|E} := \left\{ q \in \left[H^1(E) \cap C^0(E) \right] : \Delta q = 0 \text{ in } E,\ q|_e \in \mathcal{P}_1(e), \forall e \in \partial E \right\} \tag{9}$$

$\mathcal{Q}_{h|E}$ is scalar value-based functional space for the phase field variable d, while the extension towards vectorial space for displacement field $\boldsymbol{u}$ is straightforward, such as:

$$\mathcal{V}_{h|E} := \left\{ \boldsymbol{v} \in \left[H^1(E) \cap C^0(E) \right]^2 : \Delta \boldsymbol{v} = 0 \text{ in } E,\ \boldsymbol{v}|_e \in [\mathcal{P}_1(e)]^2, \forall e \in \partial E \right\} \tag{10}$$

Δ represents the component-wise Laplacian operator. $\mathcal{P}_1(e)$ represents the polynomial space of degree ≤ 1 defined on e. $\mathcal{Q}_{h|E}$ and $\mathcal{V}_{h|E}$ contain the continuous harmonic functions of which piece-wise linear on e and vanishing Laplacian interior E. The 'virtual' means that the space is well defined on the boundary of the element but not explicitly known inside the element. The spaces $\mathcal{Q}_{h|E}$ and $\mathcal{V}_{h|E}$ are linearly complete, suggesting that $[\mathcal{P}_1(E)]^2 \subseteq \mathcal{V}_{h|E}$ and $[\mathcal{P}_1(E)] \subseteq \mathcal{Q}_{h|E}$. Thus, only the degree of freedom (DOF) for $\mathcal{V}_{h|E}$ and $\mathcal{Q}_{h|E}$ are taken at the vertices of E.

Providing that, values at DOFs are given and $\boldsymbol{v} \in \mathcal{V}_{h|E}$ and $q \in \mathcal{Q}_{h|E}$ are linear on e, the value of $\boldsymbol{v}$ and q are completely known on the boundary of E. By virtue of the Gauss divergence theorem and integrating by part, one can

calculate the integral average of gradient, such as:

$$\begin{cases} \dfrac{1}{|E|}\displaystyle\int_E \nabla \boldsymbol{v}\,\mathrm{d}V = \dfrac{1}{|E|}\sum_{e\in\partial E}\int_e \boldsymbol{v}\otimes\boldsymbol{n}_e\,\mathrm{d}S = \dfrac{1}{2|E|}\sum_{j=1}^{n_V}\boldsymbol{v}\left(\boldsymbol{x}_j\right)\cdot\left(\left|e_{j-1}\right|\boldsymbol{n}_{j-1}+\left|e_j\right|\boldsymbol{n}_j\right) \\ \dfrac{1}{|E|}\displaystyle\int_E \nabla q\,\mathrm{d}V = \dfrac{1}{|E|}\sum_{e\in\partial E}\int_e q\otimes\boldsymbol{n}_e\,\mathrm{d}S = \dfrac{1}{2|E|}\sum_{j=1}^{n_V} q\left(\boldsymbol{x}_j\right)\cdot\left(\left|e_{j-1}\right|\boldsymbol{n}_{j-1}+\left|e_j\right|\boldsymbol{n}_j\right) \end{cases} \tag{11}$$

where $|e_j|$ is the length of the j-th edge and $\boldsymbol{n}_j$ represents the outward unit normal vector at each edge j. Concerning the edge indexing, for $j = 1$ and $j = n_V$, the indexes are denoted as $j-1 = n_V$ and $j+1 = 1$, respectively.

VEM relies on the split of primary variable $\mathfrak{U}$ defined in Eq.(8) into a polynomial space representation $\mathfrak{U}_{\Pi}$ and a reminder, as

$$\mathfrak{U}_h = \mathfrak{U}_{\Pi} + (\mathfrak{U}_h - \mathfrak{U}_{\Pi}) \qquad \text{with} \qquad \mathfrak{U}_{\Pi} := \{\boldsymbol{u}_{\Pi}, d_{\Pi}\} \tag{12}$$

where $\mathfrak{U}_{\Pi}$ is obtained by projecting the primary variable $\mathfrak{U}_h$ onto a polynomial space, in this case, $\mathcal{P}_1$. $\mathfrak{U}_{\Pi}$ is defined element-wise such as $\mathfrak{U}_{\Pi|E} = \{\mathfrak{U}_{\Pi,1}, \mathfrak{U}_{\Pi,2}, ...\mathfrak{U}_{\Pi,n_V}\}^T_{|E}$ and guarantees the linear consistency. The remainder term $\mathfrak{U}_h - \mathfrak{U}_{\Pi}$ guarantees the stability in VEM. For $E \in \Omega_h$, the projected primary variables satisfy that:

$$\begin{cases} \dfrac{1}{|E|}\displaystyle\int_E \nabla\mathfrak{U}_{\Pi}\,\mathrm{d}V \overset{\downarrow}{=} \dfrac{1}{|E|}\int_E \nabla\mathfrak{U}_h\,\mathrm{d}V, \\ \dfrac{1}{n_V}\displaystyle\sum_{j=1}^{n_V}\mathfrak{U}_{\Pi}(\boldsymbol{x}_j) \overset{\downarrow}{=} \dfrac{1}{n_V}\sum_{j=1}^{n_V}\mathfrak{U}_h(\boldsymbol{x}_j) \end{cases} \tag{13}$$

The calculation of projection operators and related procedure to construct the stiffness matrix and mass matrix will not be addressed here, interested readers may refer to Liu (2023) for further details.

3. Numerical examples

Table 2: Material and model parameters in all simulations.

Parameters	Three point bending test	L-shaped panel test
Young's modulus [GPa]	43.6	25.85
Poison ratio [-]	0.2	0.18
Fracture energy [N/mm]	0.1195	0.095
Length scale [mm]	10	3.125
Thickness [mm]	127	100
Crack driving force	Rankine splitting	Spectral splitting
Strain & stress state	Plane stress	Plane strain

3.1. Three point bending test

In this sub-section, the three point bending test is firstly considered, which is a well-known benchmark problem for testing the performance of phase field modeling of brittle fracture. The geometry configuration and boundary conditions are given in Fig.3(a). The notched beam is simply supported at its right end and clamped at its left end. A vertical displacement $u_y^* = 0.44$mm is applied to the loading platen on the top of the beam, where the reaction forces are recorded at the same position. The prescribed displacement is equally applied in 100 loading steps, i.e., $\Delta u_y^* = 0.044$mm. The Voronoi mesh for VEM calculation is shown in Fig.3(b), which consists of 14436 elements and 28884 nodes.The mesh is pre-refined within the expected fracture process zone, with a refined mesh size $h_E \leq l/5$. The material property and model parameters are given in the second column of Table3, which are considered in Mandal (2019) and Mosler (2004). The length scale parameter l is considered as material property determined by using 1D analytical formulation given in Wu and Nguyen (2018). However, the length scale sensitivity study is not considered, which beyonds the scope of this work.

The ultimate phase field profiles are shown in Fig.5, where FEMQ4, VEMQ4 and VEMVO give identical crack patterns. The crack initiates at the notch tip and then propagates vertically towards the top of the beam along the symmetry axis, which behaves a purely mode I crack pattern. The final phase field profiles are in good agreement with Mandal (2019), in which FEMQ4 is adopted and mesh basis analysis was studied.

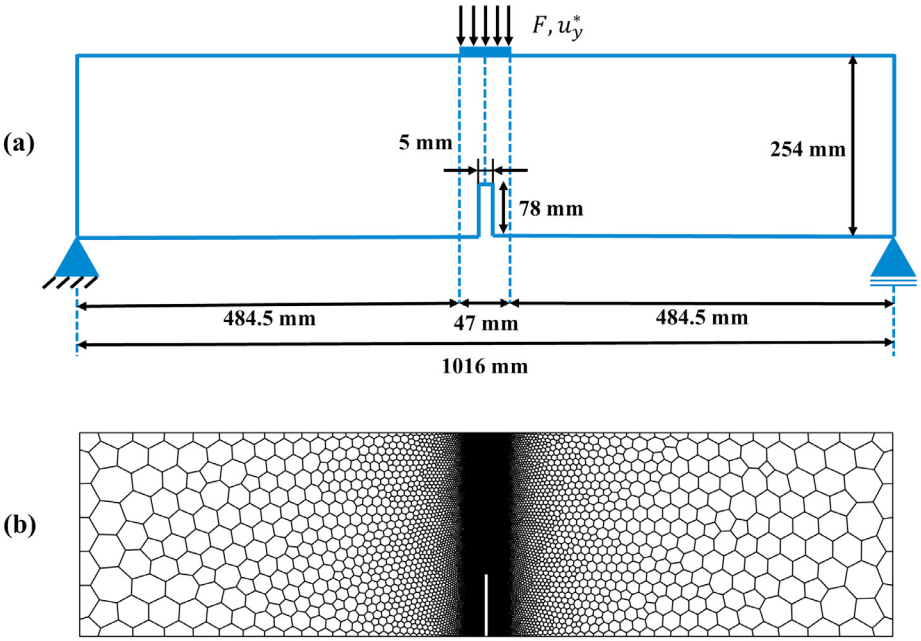

Figure 3: Three point bending test: (a): Geometry description and boundary conditions (b): Voronoi mesh for VEMVO.

The reaction force *vs* applied displacement is shown in Fig.4. The beam exhibits an elastic stage initially and fails due to the crack initiation at about $u_y^* = 0.16$mm. The loading-displacement curves of FEMQ4, VEMQ4 and VEMVO are in fairly good agreement with FEM calaulation in Mandal et al. Meanwhile, the loading threshold (26.6~26.7 kN) is captured identically between VEM and FEM calculation. The result of VEMQ4 gives the identical loading-displacement response as in FEMQ4, which shows the accuracy of proposed formulation. However, the usage of Voronoi mesh in VEMVO results in a underestimation of the initial elastic stiffness, this phenomena also exhibits in Aldakheel (2018) for a *standard* (AT2) phase field model. The comparison of CPU time as well as memory con-

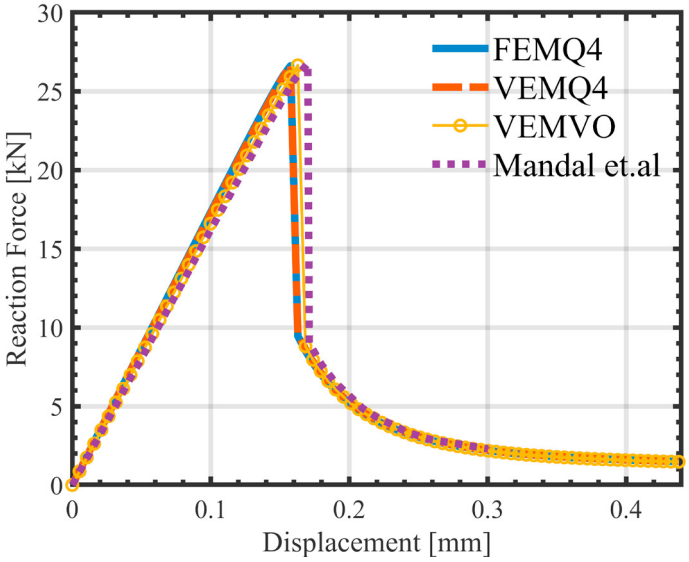

Figure 4: Three point bending test: Loading displacement curve via different methods.

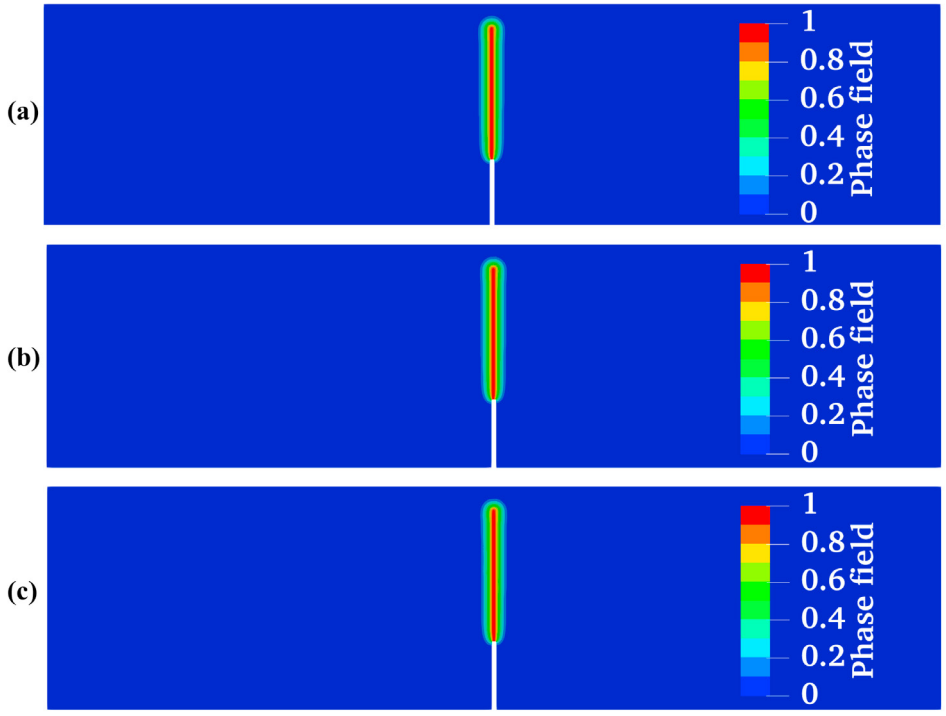

Figure 5: Three point bending test: phase field profile at $u_y^* = 0.044$mm. (a): FEMQ4, (b): VEMQ4, (c): VEMVO.

sumption between VEMQ4 and FEMQ4 will not be addressed here, interested readers may refer to Liu (2023) and Aldakheel (2018) for further reading.

3.2. L-shaped panel test (corner singularity)

In this sub-section, L-shaped panel test is considered, which is a well-known benchmark problem to test the mixed-mode type of failure Mesgarnejad (2015). The geometry descriptions and boundary conditions are presented in Fig.6 (left), which are adopted from Lampron (2021); Mesgarnejad (2015). The bottom edge of L-shaped panel specimen is fixed and the vertical displacement $\boldsymbol{u}^* = 1$mm is applied as shown in Fig.6 (left), where the reaction force are recorded at the same position. The prescribed displacement is equally applied in 50 loading steps, i.e., $\Delta\boldsymbol{u}^* = 0.02$mm. The Voronoi mesh for VEM calculation is shown in Fig.6 (right), which consists of 47415 elements and 94840 nodes. The mesh is pre-refined within the expected fracture process zone corresponding to the experimental study Winkler (2001), with a refined mesh size $h_E \leq l/6$. The material property and model parameters are given in the third column of Table3.

The ultimate fracture phase field profiles of L-shaped panel testing are shown in Fig.7(b)(c)(d), where FEMQ4, VEMQ4 and VEMVO give identical crack patterns. The crack initiates at the corner of the specimen and then propagates with an angle at the very beginning, finally stabilizing its direction horizontally, which behaves a mixed mode crack pattern. The final phase field profiles are in very good agreement with the experimental study (see Fig.7(a)) and numerical results in Lampron (2021); Mesgarnejad (2015), in which FEMQ4 is adopted.

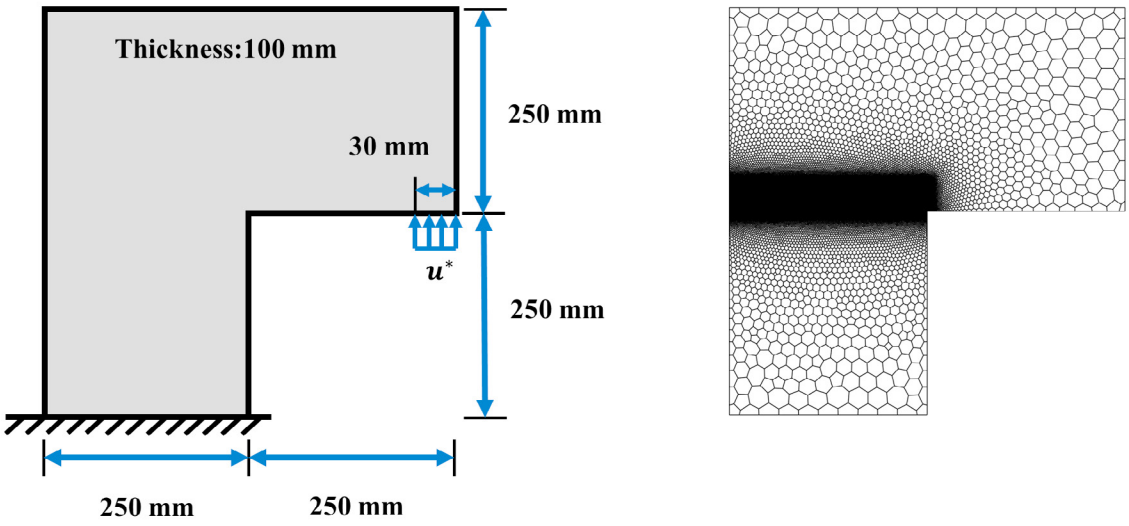

Figure 6: L-shaped panel test: Representations of geometry configuration and boundary conditions (left); Voronoi mesh discretization (right).

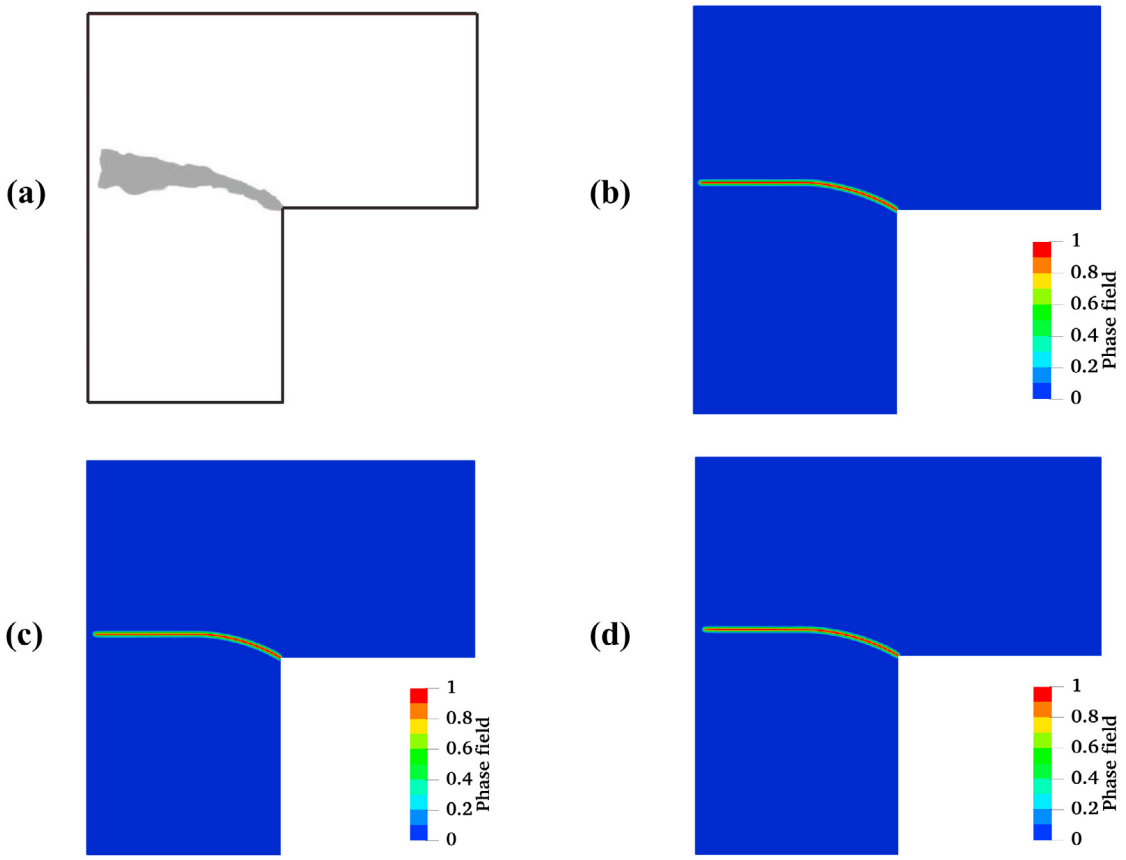

Figure 7: L-shaped panel test: phase field profile at $\boldsymbol{u}^* = 1.0$mm. (a): Experimental study, (b): FEMQ4, (c): VEMQ4, (d): VEMVO.

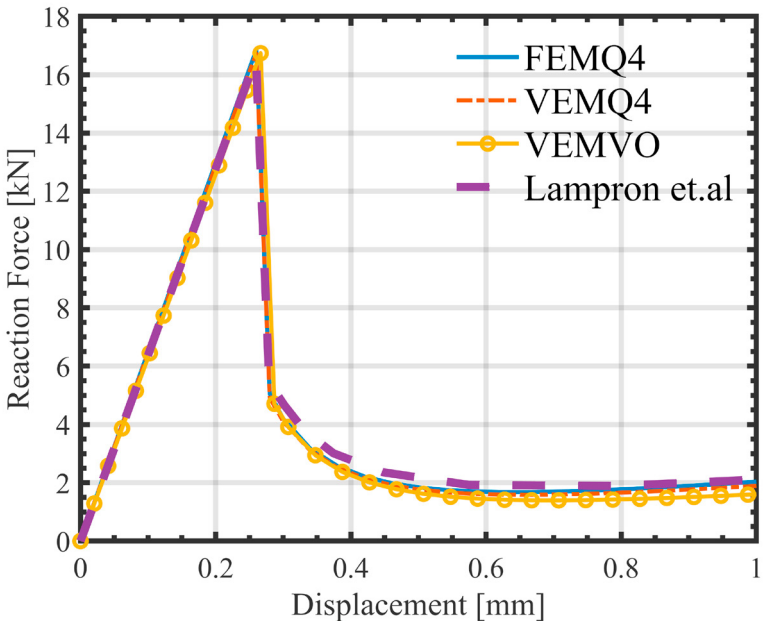

Figure 8: L-shaped panel test: loading displacement curve via different methods.

The reaction force *vs* applied displacement is presented in Fig.8. The L-shaped panel specimen exhibits an linear elastic stage initially and fails due to the crack initiation at about prescribed displacement $\boldsymbol{u}^* = 0.28$mm. The loading-displacement curves of FEMQ4, VEMQ4 and VEMVO are in very good agreement with FEM calaulation in Lampron (2021), which again shows the accuracy of proposed formulation. Meanwhile, the peak load (16.5∼16.7 kN) is captured identically between VEM and FEM calculation. Hoerver, the peak load in Lampron (2021) is slightly lower than results in this work. This is because a variational consistent phase field model is utilized, while a hybrid (variational inconsistent) scheme is adopted in this work Ambati (2015a).

4. Concluding remarks

In this work, a new and efficient virtual element formulation is proposed for *non-standard* phase field modeling of brittle fracture under quasi-static loading. Such an alternative minimization scheme is suitable for solving phase field brittle fracture problems implicitly, because the original problem is automatically decoupled into an elastostatic equation and a Poisson-type of reaction-diffusion equation. A robust bounded constraint optimization solver based on trust region reflective method Moré (1983) is used for solving damage sub-problem, which guarantees the upperbound and irreversibility of crack phase field. The performance of the proposed framework is validated by two representative benchmark problems on different choices of mesh, which indicates that the proposed VEM formulation has the capability of simulating different failure modes with accuracy, versatility, and efficiency.

Acknowledgements

This research did not receive any specific grant from funding agencies in the public, commercial, or not-for-profit sectors.

References

M. Ambati, T. Gerasimov, L. De Lorenzis, 2015. A review on phase-field models for brittle fracture and a new fast hybrid formulation. Computational Mechanics 55, 383-405

M. Ambati, T. Gerasimov, L. De Lorenzis, 2015. Phase-field modeling of ductile fracture. Computational Mechanics 55, 1017-1040

M. J. Borden, C. V. Verhoosel, M. A. Scott, T. J. R. Hughes, C. M. Landis 2012. A phase-field description of dynamic brittle fracture. Computer Methods in Applied Mechanics and Engineering 217, 77-95

C. Miehe, M. Hofacker, F. Welschinger, 2010. A phase field model for rate-independent crack propagation: Robust algorithmic implementation based on operator splits. Computer Methods in Applied Mechanics and Engineering 199, 45-48

C. Miehe, F. Welschinger, M. Hofacker,2010. Thermodynamically consistent phase-field models of fracture: Variational principles and multi-field FE implementations. International journal for numerical methods in engineering 83(10), 1273-1311

C. Miehe, L.-M. Schaenzel, H. Ulmer,2015. Phase field modeling of fracture in multi-physics problems. Part I. Balance of crack surface and failure criteria for brittle crack propagation in thermo-elastic solids. Computer Methods in Applied Mechanics and Engineering 294, 449-485

C. Miehe, M. Hofacker, L.-M. Schaenzel, F. Aldakheel,2015. Phase field modeling of fracture in multi-physics problems. Part II. Coupled brittle-to-ductile failure criteria and crack propagation in thermo-elastic–plastic solids. Computer Methods in Applied Mechanics and Engineering 294, 486-522

R. De Borst, 2022. Fracture and damage in quasi-brittle materials: A comparison of approaches. Theoretical and Applied Fracture Mechanics 122, 103652.

G. A. Fracfort, J. J. Marigo, 1998. Revisiting brittle fracture as an energy minimization problem. Journal of the Mechanics and Physics of Solids 46(8), 1319–1342.

B. Bourdin, G. A. Fracfort, J. J. Marigo, 2000. Numerical experiments in revisited brittle fracture. Journal of the Mechanics and Physics of Solids 48(4), 797–826.

J.-Y. Wu, 2017. A unified phase-field theory for the mechanics of damage and quasi-brittle failure. Journal of the Mechanics and Physics of Solids 103, 72–99.

J.-Y. Wu, V. P. Nguyen 2018. A length scale insensitive phase-field damage model for brittle fracture. Journal of the Mechanics and Physics of Solids 119, 20–42.

J.-Y. Wu et al, 2017. Phase-field modeling of fracture. Advances in applied mechanics 53, 1–183.

L. Beirão da Veiga et al, 2013. Basic principles of virtual element methods. Mathematical Models and Methods in Applied Sciences 23(1), 199-214.

L. Beirão da Veiga et al, 2014. The hitchhiker's guide to the virtual element method. Mathematical Models and Methods in Applied Sciences 24(8), 1541-1573.

L. Beirão da Veiga et al, 2015. A Virtual Element Method for elastic and inelastic problems on polytope meshes. Computer Methods in Applied Mechanics and Engineering 295, 327-346.
L. Beirão da Veiga et al, 2016. Virtual element method for general second-order elliptic problems on polygonal meshes. Mathematical Models and Methods in Applied Sciences 26(4), 729-750.
F. Aldakheel et al, 2018. Phase-field modeling of brittle fracture using an efficient virtual element scheme. Computer Methods in Applied Mechanics and Engineering 341, 443-466.
F. Aldakheel et al, 2019. Virtual element formulation for phase-field modeling of ductile fracture. International Journal for Multiscale Computational Engineering 2019, 181-200.
T.-R. Liu, F. Aldekheel, M. H. Aliabadi, 2023. Virtual element method for phase field modeling of dynamic fracture. Computer Methods in Applied Mechanics and Engineering 411, 116050.
K. Pham et al, 2009. Gradient damage models and their use to approximate brittle fracture. International Journal of Damage Mechanics 20(4), 618-652.
T. K. Mandal,V. P. Nguyen, J.-Y. Wu, 2020. Evaluation of variational phase-field models for dynamic brittle fracture. Enegineering Fracture Mechanics 235, 107169.
T. K. Mandal,V. P. Nguyen, J.-Y. Wu, 2021. Comparative study of phase-field damage models for hydrogen assisted cracking. Theoretical and Applied Fracture Mechanics 111, 102840.
T. K. Mandal,V. P. Nguyen, J.-Y. Wu, 2019. Length scale and mesh bias sensitivity of phase-field models for brittle and cohesive fracture. Enegineering Fracture Mechanics 217, 106532.
E. Martínez-Pañeda, A. Golahmar, C. Niordson, 2018. A phase field formulation for hydrogen assisted cracking. Computer Methods in Applied Mechanics and Engineering 342, 742-761.
O. Lampron, D. Therriault, M. Lévesque, 2021. An efficient and robust monolithic approach to phase-field quasi-static brittle fracture using a modified Newton method. Computer Methods in Applied Mechanics and Engineering 386, 114091.
A. Mesgarnejad, B. Bourdin, M. Khonsari, 2015. Validation simulations for the variational approach to fracture. Computer Methods in Applied Mechanics and Engineering 290, 420-437.
T. Belytschko, Y. Y. Lu, L. Gu,1994. Element-free Galerkin methods. International journal for numerical methods in engineering 37(2), 229-256
D. Sulsky, Z. Chen, H. L. Schreyer, 1994. A particle method for history-dependent materials. Computer Methods in Applied Mechanics and Engineering 118(1-2), 179-196.
J. Mosler, G. Meschke, 2004. Embedded crack vs. smeared crack models: a comparison of elementwise discontinuous crack path approaches with emphasis on mesh bias. Computer Methods in Applied Mechanics and Engineering 193(30–32), 3351-3375.
B. J. Winkler, 2001. Traglastuntersuchungen von unbewehrten und bewehrten betonstrukturen auf der grundlage eines objektiven werkstoffgesetzes für beton. (PhD thesis).
A. L. Gain, C. Talischi, G. H. Paulino, 2014. On the virtual element method for three-dimensional linear elasticity problems on arbitrary polyhedral meshes. Computer Methods in Applied Mechanics and Engineering 282, 132-160.
V. M. Nguyen-Thanh et al, 2018. A Virtual Element Method for 2D linear elastic fracture analysis. Computer Methods in Applied Mechanics and Engineering 340, 366-395.
A. Hussein, B. Hudobivnik, P. Wriggers, 2020. A Virtual Element Method for 2D linear elastic fracture analysis. Computer Methods in Applied Mechanics and Engineering 372, 113329.
J. J. Moré, D.C. Sorensen, 1983. Computing a Trust Region Step. SIAM Journal on Scientific and Statistical Computing 3, 553–572.